INTERNATIONAL JOURNAL FOR NUMERICAL METHODS IN FLUIDS, VOL. 23, 1117–1132 (1996)

FINITE ELEMENT MODELLING OF FREE SURFACE VISCOELASTIC FLOWS WITH PARTICULAR APPLICATION TO RUBBER MIXING

J. PETERA AND V. NASSEHI

Chemical Engineering Department, Loughborough University of Technology, Loughborough LE11 3TU, U.K.

SUMMARY

Internal mixers are used extensively in industry for mixing the components of rubber compounds. In these operations, in order to achieve effective mixing, the mixer chamber is always partially filled. This inevitably results in the appearance of multiple free surfaces in flow fields inside rubber mixer chambers. Mathematical modelling of such a flow regime is not a simple task and requires a great deal of effort. Traditional free surface flow-modelling techniques, which are mainly based on the use of volume-of-fluid or pseudo-density approaches in an Eulerian framework, are not flexible enough to cope with this problem. In this paper we describe a new method for the numerical modelling of free surface flows. In this method the pseudo-density approach is extended to a special Lagrangian framework along the trajectories of the fluid particles. We show that the developed scheme can very effectively simulate viscoelastic free surface flows encountered in rubber-mixing processes.

KEY WORDS: rubber mixing; free surface flows; viscoelastic flow; pseudo-density method; Lagrangian framework

INTRODUCTION

Batch internal mixers are extensively used to mix natural or synthetic rubbers with particulate fillers such as carbon black and other additives. The mixing process is an important part in the manufacture of rubber compounds with desirable properties. To achieve efficient mixing, internal mixers are always used partially filled, with fill factors sometimes as low as 60 per cent of the total mixer volume. The resulting flow inside the rubber mixer is thus a free surface regime. Therefore the mathematical modelling of rubber mixing depends on the successful simulation of a viscoelastic flow field with random free surfaces.

The first technique which was extensively used to model free surface flow regimes, associated with processes such as mould filling and metal casting, was based on an approach known as the volume-of-fluid (VOF) method. The original technique was developed in Los Alamos Scientific Laboratories (U.S.A.) and is the basis of the well-known SOLA-VOF package.[1] Other investigators have extended the method and applied it to a variety of problems.[2,3] The VOF technique uses the finite difference method and its application in problems involving complicated geometries is not straightforward. An alternative version of this method based on the finite element technique has also been developed. Owing to the complicated nature of the volume-of-fluid method, however, the finite element version of it is only applied to solve simple problems.[4]

CCC 0271–2091/96/111117–16 *Received February 1995*

Another technique which has been developed in recent years is based on treating a free surface flow field as a two-phase system. In such a system the fluid-filled regions are assumed to be one phase and the rest of the flow domain, separated by the free surface boundary, is considered as another phase. In order to model a flow field in this way, artificial physical parameters must be used outside the real fluid phase and thus the scheme is called the pseudo-density method.[5] From a practical point of view the pseudo-density method offers more flexibility than the VOF scheme, but its effectiveness is restricted by the necessity of using artificial physical parameters for void sections of the domain. An additional problem in the pseudo-density method is the numerical instability caused by the use of arbitrary artificial physical parameters. In any given problem these values should be selected after trial-and-error procedures in order to avoid unstable solutions.

In both the above-mentioned techniques a surface location function is defined and in conjunction with the flow equations an additional transport equation in terms of this function is solved. Essentially the surface location equation describes the movement and deformation of the free surface and is a pure convection equation (i.e. a hyperbolic PDE). In general in an Eulerian framework the numerical solution of the hyperbolic equations results in oscillatory solutions unless some artificial damping technique is used. The use of artificial damping methods reduces the accuracy of the obtained results and it is desirable to develop methods which avoid such a necessity.

In this paper we describe a free surface flow-modelling technique which is based on the finite element solution of the model equations in a Lagrangian framework defined along the trajectories of the fluid particles. The main advantage of this method is that since we are using a Lagrangian framework, the convection terms in the model equations are eliminated and especially the free surface location equation is reduced to a simple time derivative. Thus the solution of the free surface function equation in our model only requires an updating of the previous position of the free surface along the trajectories of the fluid particles. The novel aspect of our model is that we do not treat the flow domain as a two-phase system and only parts of the flow field which are full of fluid at any given time are included in the solution scheme. Thus there is no need to use artificial physical parameters in this method. The applicability and accuracy of the technique are demonstrated by comparisons between simulated results and experimentally observed free surfaces in a flow rig which is analogous to an internal rubber mixer.

MATHEMATICAL MODEL

Consider a two-dimensional flow field. Using an Eulerian co-ordinate system (x, y), in the absence of body forces the components of the equation of motion representing the transient creeping flow of an incompressible fluid are given by

$$\rho \frac{\partial v_x}{\partial t} = -\frac{\partial p}{\partial x} + \frac{\partial \tau_{xx}}{\partial x} + \frac{\partial \tau_{yx}}{\partial y}, \qquad \rho \frac{\partial v_y}{\partial t} = -\frac{\partial p}{\partial y} + \frac{\partial \tau_{xy}}{\partial x} + \frac{\partial \tau_{yy}}{\partial y}, \tag{1}$$

where ρ is the constant fluid density, v_x and v_y are the components of the velocity vector, p is the pressure and τ_{xx}, etc. are the components of the extra stress tensor.

The continuity equation for this type of flow is normally given by the expression of a divergence-free velocity field. In the present work, however, the following equation, which represents the mass continuity for a slightly compressible fluid, is adopted:

$$\frac{1}{c^2}\frac{\partial p}{\partial t} + \rho\left(\frac{\partial v_x}{\partial x} + \frac{\partial v_y}{\partial y}\right) = 0, \tag{2}$$

where c is the speed of sound in the fluid. The use of the above equation is more convenient, because in this case it is possible to use equal- order interpolation functions for velocity and pressure in the finite element solution scheme without violating the LBB stability condition.[6]

In the present model the components of the constitutive equation associated with the flow of a viscoelastic fluid such as rubber are given by

$$\begin{aligned}
\lambda\left(\frac{\partial T_{xx}}{\partial t}+v_x\frac{\partial T_{xx}}{\partial x}+v_y\frac{\partial T_{xx}}{\partial y}-2\frac{\partial v_x}{\partial x}T_{xx}-2\frac{\partial v_x}{\partial y}T_{xy}\right)+T_{xx}&=\frac{\mu}{\lambda},\\
\lambda\left(\frac{\partial T_{yy}}{\partial t}+v_x\frac{\partial T_{yy}}{\partial x}+v_y\frac{\partial T_{yy}}{\partial y}-2\frac{\partial v_y}{\partial x}T_{xy}-2\frac{\partial v_y}{\partial y}T_{yy}\right)+T_{yy}&=\frac{\mu}{\lambda},\\
\lambda\left(\frac{\partial T_{xy}}{\partial t}+v_x\frac{\partial T_{xy}}{\partial x}+v_y\frac{\partial T_{xy}}{\partial y}-\frac{\partial v_y}{\partial x}T_{xx}-\frac{\partial v_x}{\partial y}T_{yy}\right)+T_{xy}&=0,
\end{aligned} \tag{3}$$

where λ is the Maxwell relaxation time and T_{xx}, etc. are the components of the Maxwell stress

$$\mathbf{T}=\frac{\mu}{\lambda}\boldsymbol{\delta}+\boldsymbol{\tau}. \tag{4}$$

The total stress in the flow field is thus given by

$$\boldsymbol{\sigma}=-p\boldsymbol{\delta}+\boldsymbol{\tau}, \tag{5}$$

where $\boldsymbol{\delta}$ is the unit second-order tensor. The variable fluid viscosity μ is given by the Carreau equation[7]

$$\mu=\frac{\mu_0}{[1+(\lambda\dot{\gamma})^2]^{(1-n)/2}}, \tag{6}$$

where μ_0 is the material consistency coefficient, n is a power-law index and $\dot{\gamma}$ is the strain rate given by

$$\dot{\gamma}=\left[2\left(\frac{\partial v_x}{\partial x}\right)^2+2\left(\frac{\partial v_y}{\partial y}\right)^2+\left(\frac{\partial v_x}{\partial y}+\frac{\partial v_y}{\partial x}\right)^2\right]^{1/2}. \tag{7}$$

In conjunction with equations (1)–(7) for a free surface flow we consider the free surface continuity equation

$$\frac{\partial F}{\partial t}+v_x\frac{\partial F}{\partial x}+v_y\frac{\partial F}{\partial y}=0, \tag{8}$$

where F is a material density function which has a value equal to unity in filled parts of the domain and zero outside the free surface. On the free surface itself this function has a value between zero and unity. A mathematical procedure for the determination of an optimum value for F on the free surface is described later in this paper.

All the model equations in the present work are given in an Eulerian co-ordinate system. Their finite element solution is, however, based on a new strategy which uses a combination of Eulerian and Lagrangian approaches. The Lagrangian framework in which equations (3) and (8) are solved is constructed by the determination of the fluid particle trajectories in the flow field.

DETERMINATION OF FLUID PARTICLE TRAJECTORIES

The position vector of a material point P in a flow field can be given as the function

$$\mathbf{X}=\mathbf{f}(P,t), \tag{9}$$

where t is the current time. A specific position at a chosen (reference) time identifies a particular point and we have

$$\mathbf{x} = \mathbf{f}(P, t^r). \tag{10}$$

Any single point occupies only one position at any given time and therefore the above function with respect to P is invertible, i.e.

$$P = \mathbf{f}^{-1}(\mathbf{x}, t^r). \tag{11}$$

Substituting from equation (11) into equation (9), we get

$$\mathbf{X} = \mathbf{f}[\mathbf{f}^{-1}(\mathbf{x}, t^r); t] = \tilde{\mathbf{X}}(\mathbf{x}, t^r; t). \tag{12}$$

If the current time t coincides with the reference time t^r, then the current and reference positions will also coincide and we may write

$$\tilde{\mathbf{X}}(\mathbf{x}, t^r; t^r) = \mathbf{x}. \tag{13}$$

In a given velocity field $\mathbf{u} = \mathbf{u}(\mathbf{x}, t^r)$ the motion of a material point is described by the equation

$$\frac{\mathrm{d}\mathbf{X}(\mathbf{x}, t^r; t)}{\mathrm{d}t} = \mathbf{u}[\mathbf{X}(\mathbf{x}, t^r; t), t], \tag{14}$$

for which the initial conditions are defined by equation (13). We use the described general kinematical remarks to derive a relationship for the determination of the starting points of the fluid particle trajectories in a flow field.

At a given time t_n the nth position of a material point, $\mathbf{X}^n$, is found by replacing t in equation (12) with t_n. At the next instant t_{n+1} we denote the position of the same point by $\mathbf{x}$. Thus the distance which the considered point has moved can be found by integrating equation (14) between t_n and t_{n+1}. This gives

$$\mathbf{x} - \mathbf{X}^n = \int_{t_n}^{t_{n+1}} \mathbf{u}[\mathbf{X}(t), t]\mathrm{d}t. \tag{15}$$

Using the mean value theorem for definite integrals, we get

$$\mathbf{x} - \mathbf{X}^n = \mathbf{u}[\mathbf{X}(t_\theta), t_\theta]\Delta t_n, \tag{16}$$

where $\Delta t_n = t_{n+1} - t_n$ and θ has a value between zero and unity. By Taylor series expansion the velocity function in the neighbourhood of point $(\mathbf{x}, t_n)$ is given as

$$\mathbf{u}[\mathbf{X}(t_\theta), t_\theta] = \mathbf{u}(\mathbf{x}, t_n) + \partial_t \mathbf{u}(\mathbf{x}, t_n)(t_\theta - t_n) + \nabla \mathbf{u}(\mathbf{x}, t_n)[\mathbf{X}(t_\theta) - \mathbf{x}]. \tag{17}$$

The second and third terms on the right-hand side of equation (17) are approximated using the available information at each time step by backward differences:

$$\partial_t \mathbf{u}(\mathbf{x}, t_n) \approx \frac{\mathbf{u}(\mathbf{x}, t_n) - \mathbf{u}(\mathbf{x}, t_{n-1})}{\Delta t_{n-1}}, \tag{18}$$

$$t_\theta - t_n \approx \tfrac{1}{2}\Delta t_n, \tag{19}$$

$$\mathbf{X}(t_\theta) - \mathbf{x} \approx \tfrac{1}{2}[\mathbf{X}(t_n) - \mathbf{x}]. \tag{20}$$

We substitute from equations (18)–(20) into equation (17) and then in turn we substitute the resulting relationship into equation (16). After rearranging, we obtain

$$\mathbf{x} - \mathbf{X} = \frac{\Delta t_n}{2}(\boldsymbol{\delta} + \tfrac{1}{2}\Delta t_n \nabla \mathbf{u}_n)^{-1}\left(\mathbf{u}_n + \tfrac{1}{2}\frac{\Delta t_n}{\Delta t_{n-1}}(\mathbf{u}_n - \mathbf{u}_{n-1})\right), \tag{21}$$

where δ is the Kronecker delta. Thus, if in a flow domain the velocity fields at times t_{n-1} and t_n are known, using equation (21), the global co-ordinates (i.e. $\mathbf{X}$) of individual starting points of fluid particle trajectories passing through fixed points with given co-ordinates ($\mathbf{x}$) can be found. In practice these fixed positions are selected to correspond to those nodal points where we wish to obtain the flow field data.

SOLUTION STRATEGY

The solution strategy used in the present work can be summarized by the following steps.

Step 1

The entire domain of interest is first discretized into a mesh of finite elements in the normal manner. This mesh is called the 'fixed mesh'. In the fixed mesh those elements which include at least one 'active node' are said to be active. The mesh of all active elements is called the 'current flow domain' (Figure 1). The active nodes are those for which $0{\cdot}4 \leqslant F \leqslant 1$, where F is the free surface function described by equation (8). The upper limit of this function is chosen by definition and the reason for choosing 0·4 as its lower limit is explained later.

Step 2

Using the fixed mesh data, an array is prepared which includes the numbers of all elements containing a given node. We call this array the 'location array'. The numbers of nodes located on the exterior boundary of the fixed mesh are also stored in a separate array called the 'boundary node array'.

Step 3

A set of appropriate initial values for the velocity, pressure and extra stress fields is assumed. At this stage the entire domain is considered (i.e. the current flow domain is the same as the fixed mesh) and the initial conditions are given in all nodal points.

Step 4

The time variable is updated, incrementing it by Δt.

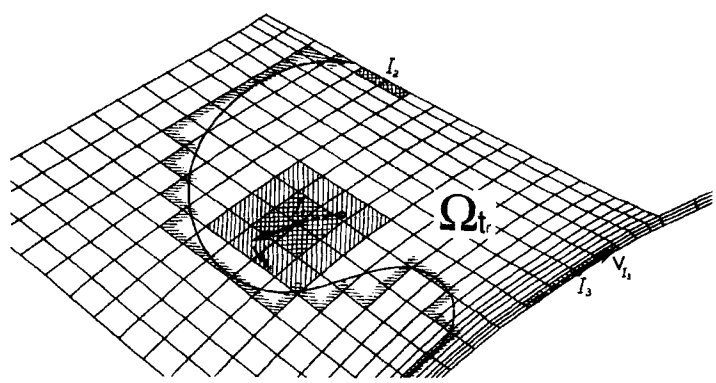

Figure 1. Current flow domain, active elements and examples of fluid particle paths

Step 5

Flow equations (1) and (2) are solved on the current domain to obtain the current values of the velocity and pressure fields, using the old time step values of the extra stress field. We use a modified version of the Taylor–Galerkin method to carry out this step.

Step 6

Using the co-ordinates of the nodal points in the current flow domain ($\mathbf{x}$), the velocity field obtained in Step 4 ($\mathbf{u}_n$) and the old velocity values ($\mathbf{u}_{n-1}$), the starting points of the fluid particle trajectories ($\mathbf{X}(t_n)$) (called feet) passing through the nodal points are found via equation (21).

Step 7

For each interior node in the current flow domain (i.e. those nodes which are not on the boundary of the fixed mesh) the location array is searched to find inside which element the foot of the fluid particle trajectory passing through it (found in Step 6) is located.

The search procedure is based on the solution of the set of non-linear algebraic equations

$$\mathbf{X} = \sum_I N_I(\xi, \eta)\mathbf{x}_I. \tag{22}$$

The unknowns here are the local co-ordinates of the foot. Thus, by inserting the found global co-ordinates of the foot in the left-hand side of equation (22) and the global co-ordinates of the nodal points of a given element in the right-hand side of equation (22), a set of 2×2 non-linear equations is constructed and solved using the Newton–Raphson method. If the foot is inside the selected element, then for a quadrilateral element the values of the local co-ordinates must be between -1 and $+1$ ($-1 \leqslant \xi, \eta \leqslant +1$). For other types of elements, corresponding appropriate criteria must be adopted.

This search at first is confined to the layer of elements containing the node under consideration. If it is found that the starting point of the trajectory passing through the node is not within any of these elements, then the search is extended to the next layer adjacent to them. In the case where the trajectory's foot is not located within these next layers, then the time increment is reduced and Steps 5–7 are repeated.

Step 8

After identifying the starting points of the particle trajectories in Step 6 and the elements within which they are located in Step 7, the function F and the stresses at these feet are found by interpolating their old time step nodal values. For nodes on the exterior boundary of the 'fixed mesh' (stored in the 'boundary node array'), which may be part of the 'current flow domain', the passing trajectory may be tangential to the domain boundary (Figure 1). In this case the foot being sought will be located outside the 'fixed mesh' and instead of interpolating nodal values of F, etc., an extrapolation procedure must be used.

Step 9

The interpolated values of F and the stresses calculated in Step 8 (stresses are recalculated by converting from a fixed to a convected co-ordinate system, via equation (35) given in the next section) are used as initial conditions and current values of these unknowns are found by solving equations (3) and (8) together with the auxiliary equations (4), (6) and (7). The finite element solution technique used in this step is a new method based on the application of the Reynolds transport

theorem to derive working equations in a Lagrangian framework which corresponds to the trajectories of the fluid particles. The details of the development of the working equations of this scheme are described in the next section.

Step 10

Using updated values of the free surface function, the new active nodes are identified and the current flow domain is updated. The updating of the current flow domain is carried out by the addition of new active elements to the previous domain and the elimination of those elements which no longer contain at least one active node.

Step 11

If the current time has reached the final time required for the flow simulation, then the calculations are terminated; otherwise Steps 3–10 are repeated.

WORKING EQUATIONS OF SOLUTION SCHEME

The working equations of the present mathematical model consist of two distinct sets.

The first set is derived from the flow and continuity equations (i.e. equations (1) and (2)) in an Eulerian framework corresponding to the 'current flow domain'. We use a modified version of the previously reported Taylor–Galerkin method for slightly compressible flow[6] in which the time increment in the Taylor series expansion is chosen to be equal to $\theta\Delta t$. This selection makes the scheme flexible and, by using different values of $0 \leqslant \theta \leqslant 1$, we can control the amount of upwinding required for smooth solutions. The derivation procedure for this set is routine and here we only give the final forms of the working equations representing the momentum and continuity equations:

$$\mathbf{M}_{I,J}^{n+1}\begin{bmatrix} U_J \\ V_J \\ P_J \end{bmatrix}^{n+1} = \mathbf{M}_{I,J}^{n}\begin{bmatrix} U_J \\ V_J \\ P_J \end{bmatrix} + \mathbf{B}_I^n, \tag{23}$$

where

$$\mathbf{M}_{I,J}^{n+1} = \begin{bmatrix} \int_\Omega (N_I N_J + \frac{1}{2}\Delta t^2 c^2 \theta N_{I,1} N_{J,1})\mathrm{d}\Omega & \int_\Omega (\frac{1}{2}\Delta t^2 c^2 \theta N_{I,1} N_{J,2})\mathrm{d}\Omega & \int_\Omega (-\Delta t \theta N_{I,1} N_J)\mathrm{d}\Omega \\ \int_\Omega (\frac{1}{2}\Delta t^2 c^2 \theta N_{I,2} N_{J,1})\mathrm{d}\Omega & \int_\Omega (N_I N_J + \frac{1}{2}\Delta t^2 c^2 \theta N_{I,2} N_{J,2})\mathrm{d}\Omega & \int_\Omega (-\Delta t \theta N_{I,2} N_J)\mathrm{d}\Omega \\ \int_\Omega (-\Delta t \theta N_I N_{J,1})\mathrm{d}\Omega & \int_\Omega (-\Delta t \theta N_I N_{J,2})\mathrm{d}\Omega & \int_\Omega [-(1/c^2) N_I N_J - \frac{1}{2}\Delta t^2 \theta (N_{I,1} N_{J,1} + N_{I,2} N_{J,2})]\mathrm{d}\Omega \end{bmatrix}, \tag{24}$$

$$\mathbf{M}_{I,J}^{n} = \begin{bmatrix} \int_\Omega [N_I N_J - \frac{1}{2}\Delta t^2 c^2 (1-\theta) N_{I,1} N_{J,1}]\mathrm{d}\Omega & \int_\Omega [-\frac{1}{2}\Delta t^2 c^2 (1-\theta) N_{I,1} N_{J,2}]\mathrm{d}\Omega & \int_\Omega [\Delta t (1-\theta) N_{I,1} N_J]\mathrm{d}\Omega \\ \int_\Omega [-\frac{1}{2}\Delta t^2 c^2 (1-\theta) N_{I,2} N_{J,1}]\mathrm{d}\Omega & \int_\Omega [N_I N_J - \frac{1}{2}\Delta t^2 c^2 (1-\theta) N_{I,2} N_{J,2}]\mathrm{d}\Omega & \int_\Omega [\Delta t (1-\theta) N_{I,2} N_J]\mathrm{d}\Omega \\ \int_\Omega [\Delta t (1-\theta) N_I N_{J,1}]\mathrm{d}\Omega & \int_\Omega [\Delta t (1-\theta) N_I N_{J,2}]\mathrm{d}\Omega & \int_\Omega [-(1/c^2) N_I N_J + \frac{1}{2}\Delta t^2 (1-\theta)(N_{I,1} N_{J,1} + N_{I,2} N_{J,2})]\mathrm{d}\Omega \end{bmatrix}, \tag{25}$$

$$\mathbf{B}_I^n = \begin{bmatrix} \int_\Omega [-(N_{I,1}\tau_{11}^n + N_{I,2}\tau_{12}^n)\Delta t]\mathrm{d}\Omega \\ \int_\Omega [-(N_{I,1}\tau_{12}^n + N_{I,2}\tau_{22}^n)\Delta t]\mathrm{d}\Omega \\ \int_\Omega -\frac{1}{2}\Delta t^2 \left[N_{I,1}\left(\frac{\partial \tau_{11}^n}{\partial x_1} + \frac{\partial \tau_{12}^n}{\partial x_2}\right) + N_{I,2}\left(\frac{\partial \tau_{12}^n}{\partial x_1} + \frac{\partial \tau_{22}^n}{\partial x_2}\right)\right]\mathrm{d}\Omega \end{bmatrix}. \tag{26}$$

The second set of working equations in the present model is derived using a Lagrangian approach. We first consider equation (8) which gives the location of the free surface in terms of the contours of F, the material density function. In order to develop a Galerkin finite element solution for this equation in a moving mesh, we start with the time derivative

$$\frac{\mathrm{d}}{\mathrm{d}t}\int_{\Omega_t} N_I F \mathrm{d}\Omega, \tag{27}$$

where Ω_t describes a moving solution domain which changes with respect to time and

$$F = \sum N_J F_J. \tag{28}$$

Using the Reynolds transport theorem, the above integral can be written as

$$\frac{\mathrm{d}}{\mathrm{d}t}\int_{\Omega_t} N_I F \mathrm{d}\Omega_t = \int_{\Omega_t}\left(\frac{\mathrm{D}N_I}{\mathrm{D}t}F + N_I\frac{\mathrm{D}F}{\mathrm{D}t}\right)\mathrm{d}\Omega_t + \int_{\Omega_t} N_I F \nabla\cdot\mathbf{u}\mathrm{d}\Omega_t. \tag{29}$$

On the RHS of equation (29) the first integral describes the changes with time in the function itself and the second integral is representative of changes due to the movement of the solution domain. As explained in the previous section, in the present scheme the deformation of the mesh and the changes in the function F along the predetermined particle trajectories are considered. Every fluid particle is the same along its trajectory and N_I, which is a geometrical function and does not explicitly depend on time, remains unchanged in a convective framework. Therefore $\mathrm{D}N_I/\mathrm{D}t = 0$, and since $\mathrm{D}F/\mathrm{D}t = 0$ (equation (8)) and $\nabla\cdot\mathbf{u} = 0$ for an incompressible fluid, then equation (29) gives

$$\frac{\mathrm{d}}{\mathrm{d}t}\int_{\Omega_t} N_I F \mathrm{d}\Omega_t = 0. \tag{30}$$

After integration with respect to time we have

$$\int_{\Omega_{n+1}} (N_I F)^{n+1}\mathrm{d}\Omega_{n+1} = \int_{\Omega_n} (N_I F)^n \mathrm{d}\Omega_n. \tag{31}$$

In the finite element solution scheme the trial functions are replaced by the interpolation functions and the unknowns are given in terms of their nodal values. This leads to the derivation of the working equation corresponding to the free surface tracking in the present scheme as

$$\sum_J M_{IJ}^{n+1} F_J^{n+1} = \sum_J M_{IJ}^n \tilde{F}_J^n, \tag{32}$$

where $\tilde{F}_J^n$ is the old time step value of the material density function at the foot of the particle trajectory passing through node J at the current time step $n+1$ and

$$M_{IJ}^{n+1} = \int_{\Omega_{n+1}} N_I N_J \mathrm{d}\Omega_{n+1}, \qquad M_{IJ}^n = \int_{\Omega_n} N_I N_J \mathrm{d}\Omega_n.$$

The outlined method makes it unnecessary to modify the interpolation functions in the finite element scheme for the Lagrangian approach. This is in contrast with previously reported methods used to develop finite element solutions for fluid flow problems in Lagrangian frameworks.[8,9]

The second equation in our mathematical model which is solved in a Lagrangian framework is the rheological equation (3) which describes the stress and rate- of-strain relationships for a viscoelastic fluid. In the convected co-ordinate system adopted here the metric tensor is defined as

$$[\mathrm{d}\tilde{\mathbf{X}}(t)]^2 = \gamma_{ij}(t)\mathrm{d}l^i\mathrm{d}l^j, \tag{33}$$

with

$$\gamma_{ij} = \frac{\partial X^k}{\partial x^i}\frac{\partial X^m}{\partial x^j} g_{km}, \tag{34}$$

where g_{km} are the components of the metric of the reference co-ordinate system (for Cartesian co-ordinates $g_{km} = \delta_{km}$). Let us denote the components of the stress tensor as

$$\Pi^{ij} = \frac{\partial l^i}{\partial X^m} T^{km} \frac{\partial l^j}{\partial X^k} = \frac{\partial x^i}{\partial X^m} T^{mk} \frac{\partial x^j}{\partial X^k}. \tag{35}$$

In the convected co-ordinate system the Maxwell equation (i.e. equation (3)) can be written as[10]

$$\lambda \dot{\Pi}^{ij} + \Pi^{ij} = \frac{\mu}{\lambda}\gamma^{ij}. \tag{36}$$

The above equation shows that in the convective co-ordinate system the components of the rheological equation are decoupled. Furthermore, in contrast with the Eulerian system, the convective terms in this equation are zero. We consider the finite element weighted residual statement of equation (36),

$$\int_{\Omega_{n+1}} \lambda N_I \Pi^{ij} \mathrm{d}\Omega_{n+1} - \int_{\Omega_n} \lambda N_I \Pi^{ij} \mathrm{d}\Omega_n = \int_{t_n}^{t_{n+1}} \int_{\Omega_t} N_I \left(-\Pi^{ij} + \frac{\mu}{\lambda}\gamma^{ij}\right) \mathrm{d}\Omega_t \mathrm{d}t, \tag{37}$$

which after discretization and application of the θ-method gives the required working equation for the calculation of the stress components as

$$(M_{IJ}^{n+1} + \theta \Delta t K_{IJ}^{n+1})(\Pi^{ij})^{n+1} = [M_{IJ}^n - (1-\theta)\Delta t K_{IJ}^n](\tilde{\Pi}_J^{ij})^n + \Delta t B_I^{n+\theta}, \tag{38}$$

where

$$M_{IJ}^{n+1} = \int_{\Omega_{n+1}} \lambda N_I N_J \mathrm{d}\Omega_{n+1}, \qquad M_{IJ}^n = \int_{\Omega_n} \lambda N_I N_J \mathrm{d}\Omega_n,$$

$$K_{IJ}^{n+1} = \int_{\Omega_{n+1}} N_I N_J \mathrm{d}\Omega_{n+1}, \qquad K_{IJ}^n = \int_{\Omega_n} N_I N_J \mathrm{d}\Omega_n,$$

$$B_I^{n+\theta} = \theta \int_{\Omega_{n+1}} N_I \delta^{ij} \mathrm{d}\Omega_{n+1} + (1-\theta) \int_{\Omega_n} N_I \gamma^{ij} \mathrm{d}\Omega_n.$$

$(\tilde{\Pi}_J^{ij})^n$ is found by interpolating existing nodal values at the old time step and then transforming the found value to the convected co-ordinate system. The calculation of the components γ^{ij} and $(\tilde{\Pi}_J^{ij})^n$ involve the first-order derivatives of the co-ordinate transformation induced by the flow. This gives the measure of deformation experienced by a volume of fluid between time steps n and $n+1$ (Figure 2). In the present model the geometrical transformation is along particle trajectories, and since the local co-ordinates of a given particle are independent of time, these derivatives are thus given as

$$\frac{\partial x^i}{\partial X^j} = \frac{\partial x^i}{\partial \xi}\frac{\partial \xi}{\partial X^j} + \frac{\partial x^i}{\partial \eta}\frac{\partial \eta}{\partial X^j}. \tag{39}$$

In order to preserve the smoothness of the described transformation in the finite element solution, we need to use the interpolation functions with continuous first-order derivatives. Thus in the present work we use C^1 isoparametric Hermite elements[11–13] to satisfy this requirement. We note that for non-elastic fluids the rheological equation is much simpler and there is no need to formulate and solve separate equations for the stresses. Thus for generalized Newtonian fluids, for example, free surface flows can be very conveniently simulated with our method without using Hermite elements.

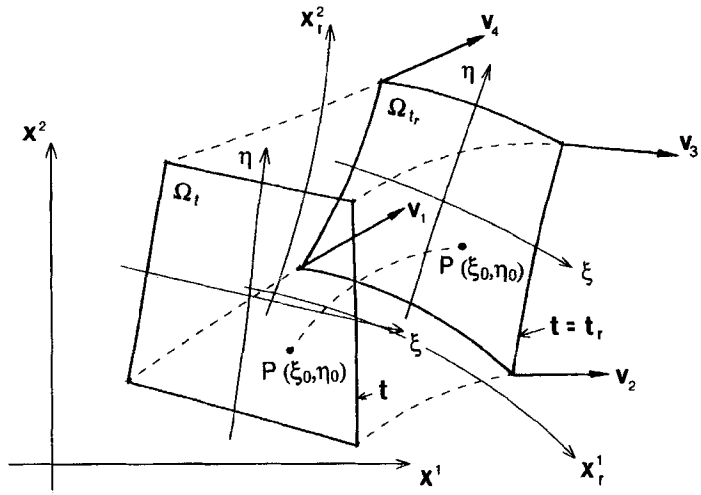

Figure 2. Co-ordinate transformation between fixed and convective systems

DETERMINATION OF OPTIMUM VALUE OF MATERIAL DENSITY FUNCTION AT FREE SURFACE

As explained previously, the location of the free surface in the present scheme is determined by the solution of equation (8) in a convective co-ordinate system. The contour corresponding to $F = 0{\cdot}4$ is the line determining the free surface boundary in the flow domain. The given value for the material density function is considered to be an optimum cut-off constant to distinguish between filled and void sections and is found in the following manner.

The main objective in free surface tracking is to determine how far the fluid front is advanced or retreated during a given time interval. This distance in any case is equal to the fluid velocity times the time interval. In a finite element context where the solution domain is discretized into elements, if this product is small in any section, then from one time step to the next the moving fluid front will still remain inside the same layer of elements. Eventually the front will move outside the current element boundaries and a new layer of active elements should be added to the current domain. Thus the number of steps, n_s, after which the current flow domain should be adjusted (by the addition or subtraction of a layer of elements) can be found as

$$n_s = \frac{h/v}{\Delta t}, \tag{40}$$

where h is the element size and v is the velocity. In a distorted non-uniform mesh with variable velocity field it is not convenient to calculate the number of steps required for mesh adjustment using the above relationship. On the other hand, the solution of the free surface equation (8) at each time step gives the nodal value of F. If the fluid is receding from a node, this value will drop; if it is advancing, the value will rise. Since the number of steps required to include (or exclude) a node and the new layer of elements to which it belongs should be equal to n_s, we need to find a value of F which satisfies the following criteria: for forward flow of the fluid,

$$F_{Cr} \leqslant F_I^{n_s} \quad \text{and} \quad F_I^{n_s-1} < F_{Cr};$$

for backward flow of the fluid,

$$F_{\mathrm{Cr}} \geq F_I^{n_s} \quad \text{and} \quad F_I^{n_s-1} > F_{\mathrm{Cr}}.$$

In the above inequalities, $F_I^{n_s}$ and $F_I^{n_s-1}$ represent respectively the values of the material density function at a boundary node I after n_s and $n_s - 1$ movements of the approaching free surface line within the element which contains that node. We elucidate this point in Figure 3, which shows part of the current domain with a free surface boundary at a given time. The value of F at node $I - 1$ in this figure at this time has exceeded its critical value and thus a new layer of elements such as the element (e) is added to the current domain. At node I the value of F at this time is zero. We consider the case when the fluid is approaching this node. After one time step the new value of F at node I is calculated. If this is less than the critical value of F, the domain at this part is kept as before and the calculations are repeated for another time interval; otherwise a new layer of elements is added to it. The number of steps which it may take to make such an adjustment necessary depends on the velocity of the fluid and the chosen time interval. A suitable value of the material density function should make the number of calculations required between successive mesh adjustments equal to n described in equation (40). The procedure to find such a constant between zero and unity is shown in Figure 3. The analogous situation for a retreating flow is shown in Figure 4.

The following analysis based on the generalization of Figures 3 and 4 yields the optimum value of F, which is the same for both flow situations.

In Figure 3 the positions of the points C, D, etc. on the F-axis correspond to the values of the material density function at node I at a given time. These values are found using interpolations in the finite element solution. Thus straight lines such as AC, which are constructed by joining similar positions for node $I - 1$ with their counterparts for node I, represent the projections of the interpolation functions on a vertical plane. After the first step of calculation of the material density function at node $I - 1$ we can write

$$\frac{F - F_{I-1}^0}{1 - F_{I-1}^0} = \frac{x - x_I}{x_{I-1} - x_I}, \tag{41}$$

which is the equation of the line O_1O_2 (Figure 3). In order to find the point A, we substitute $x_I + \delta$ for x in the above equation. Thus

$$\frac{F_{I-1}^1 - F_{I-1}^0}{1 - F_{I-1}^0} = \frac{x_I + \delta - x_I}{x_{I-1} - x_I} = \frac{\delta}{h}, \qquad h = x_{I-1} - x_I, \tag{42}$$

or

$$F_{I-1}^1 = \left(1 - \frac{1}{n}\right) F_{I-1}^0 + \frac{1}{n}, \tag{43}$$

where n is the number of steps given by equation (40) which was used to adjust the mesh at the previous time. A recurrence formula based on equation (43) is constructed:

$$F_{I-1}^k = \left(1 - \frac{1}{n}\right) F_{I-1}^{k-1} + \frac{1}{n}. \tag{44}$$

Using the formula for geometric progression, we can write

$$F_{I-1}^k = 1 - \left(1 - \frac{1}{n}\right)^k (1 - F_{I-1}^0). \tag{45}$$

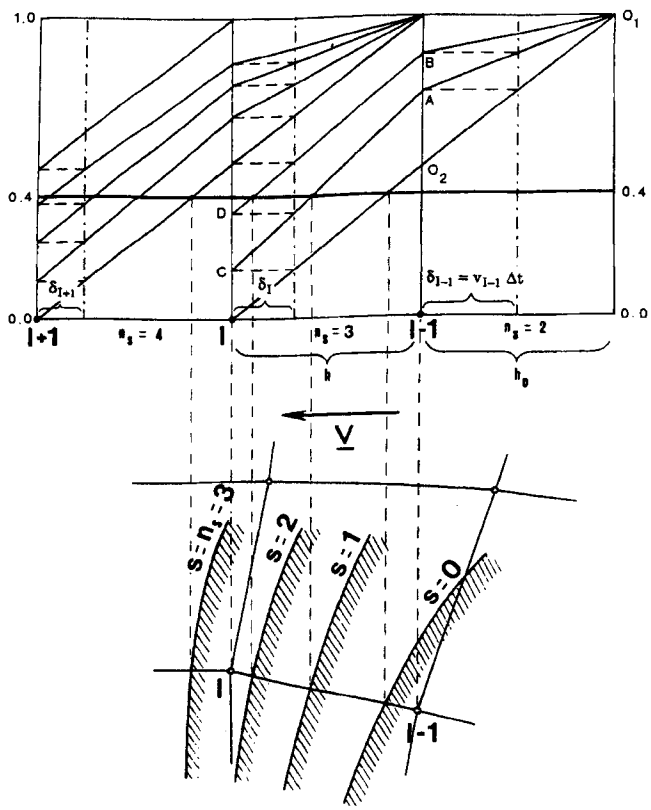

Figure 3. Forward-moving free surface with corresponding stepwise change in finite element interpolations

Similarly, for node I we write the equation of the line AC (Figure 3) at the kth step as

$$\frac{F - F_I^k}{F_{I-1}^k - F_I^k} = \frac{x - x_{I-1}}{x_I - x_{I-1}}. \tag{46}$$

Using a procedure analogous to the one given above, for a point such as C located on the current element edge we substitute the $(k+1)$th value of F into equation (46) to obtain the location of the next point on that edge. This leads to the derivation of the recurrence formula

$$F_I^{k+1} = \left(1 - \frac{1}{n_s}\right) F_I^k + \frac{1}{n_s} F_{I-1}^k. \tag{47}$$

Inserting a wide range of step numbers (n_s between 1 and 10), the positions of points A, B and C, D (Figure 3) were found from the recurrence formulae (45) and (47) respectively. Whenever $k+1$ in equation (47) becomes equal to the inserted value n_s, a new layer of elements should be added to the current domain (free surface boundary moving forward). It was found that choosing $F = 0{\cdot}4$ contours as the boundary between filled and void sections of the flow domain would always guarantee that for a step number one less than the inserted value the free surface would remain below the current flow domain edge. A similar analysis was conducted for a backward-moving free surface boundary and it

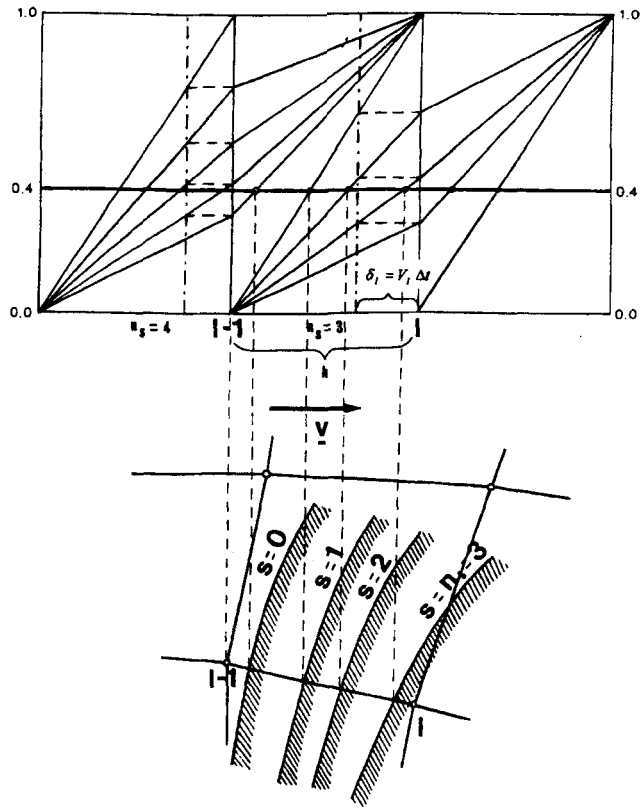

Figure 4. Backward-moving free surface with corresponding stepwise change in finite element interpolations

was again confirmed that $F = 0{\cdot}4$ should be chosen as the free surface contour value. In this case, element layers with material density function value less than 0·4 should be eliminated from the current flow domain.

COMPARISON OF NUMERICAL RESULTS AND EXPERIMENTAL DATA

In order to validate the developed model, a complex flow visualization rig was constructed. Details of this rig and the developed experimental techniques will be published separately. In this paper, only a brief account of the basic structure of the rig is given.

Essentially the experimental rig consisted of a rotating horizontal cylinder with an attached blade section. This section could be changed to provide experimental data for various types of blade geometry used in rubber mixing. The blade section had a uniform shape in the direction of the barrel axis to generate a flow domain which could be effectively considered as two- dimensional. Pressure transducers in the blade section gave the measured pressure at the tip and along the gap between the blade and barrel surfaces. The gap size between these two surfaces was adjustable. At the start of experiments the blade was moved away from the barrel and a band of rubber was wrapped around the cylinder. The blade was then brought close to the barrel surface. The flow generated by the rotation of the barrel resulted in free surface regimes before the blade tip and also at the exit from the narrow contraction. By using a video camera located at the side of the rig, free surface locations at various

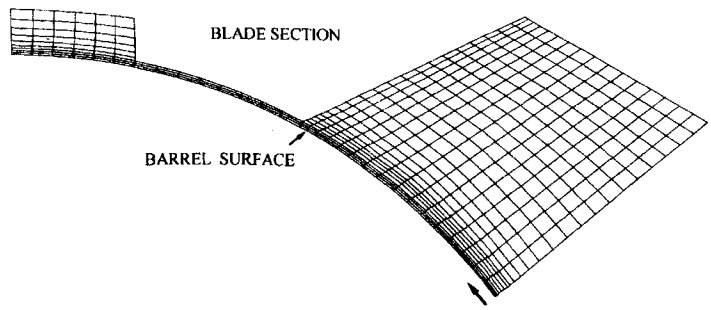

Figure 5. Eulerian mesh of maximum flow domain

times were recorded. These recordings were converted into free surface contours which can be directly compared with the model results. Figure 5 shows the finite element mesh of the maximum flow domain, which consists of a reservoir before the blade tip, a narrow gap between the blade and the barrel and a section at the exit side of the blade. The experimental rig geometry is the mirror image of a commercial internal rubber mixer and provides a complex domain for the direct comparison of numerical model results with the observed free surface locations and shapes in a viscoelastic flow field.

Numerical model results for a rubber with a consistency coefficient of 5×10^5 Pa s, a density of 1100 kg m^{-3} and a relaxation time of 0·54 s are compared with the observed free surfaces in Figures 6(a)–(d). The creeping flow of rubber observed in these experiments can be considered as isothermal. The close agreement between model results and experimental data provides confirmation of the validity of the developed scheme. The small discrepancy between model results and experimental data can be attributed to factors such as the impossibility of producing exactly two-dimensional flow regimes during the experiments. It is interesting to note that the discrepancy between two sets of results remains small and unchanged after relatively long simulation times. This is in contrast with the model results produced using a traditional pseudo-density scheme on a fixed framework. The result of such a simulation for a free surface after 55 s from the start of flow is shown in Figure 7. The large discrepancy between simulated results and experimental evidence in this case confirms the unsuitability of using the traditional method for complex viscoelastic free surface flows.

As a typical example, the simulated pressure field produced by the described model for 15 s after starting from a completely full reservoir is shown in Plate 1. The computed pressure fields, which can be used in mixer design calculations, are also in agreement with experimental observations. A full account of such a design procedure will be published separately.

CONCLUSIONS

A new technique based on the extension of the pseudo-density method to a special Lagrangian framework, constructed along the trajectories of the fluid particles, for the simulation of complicated free surface flows is presented. The developed method is applied to the simulation of an isothermal viscoelastic flow in a geometry analogous to an internal rubber mixer. The comparison between model results and experimental data confirms the validity of the adopted method. The application of the method to a non-isothermal non-elastic free surface flow presents no difficulties. The numerical simulation of a non-isothermal viscoelastic flow, however, involves complications which are independent of the free surface nature of the modelled regimes and thus is beyond the scope of the present paper.

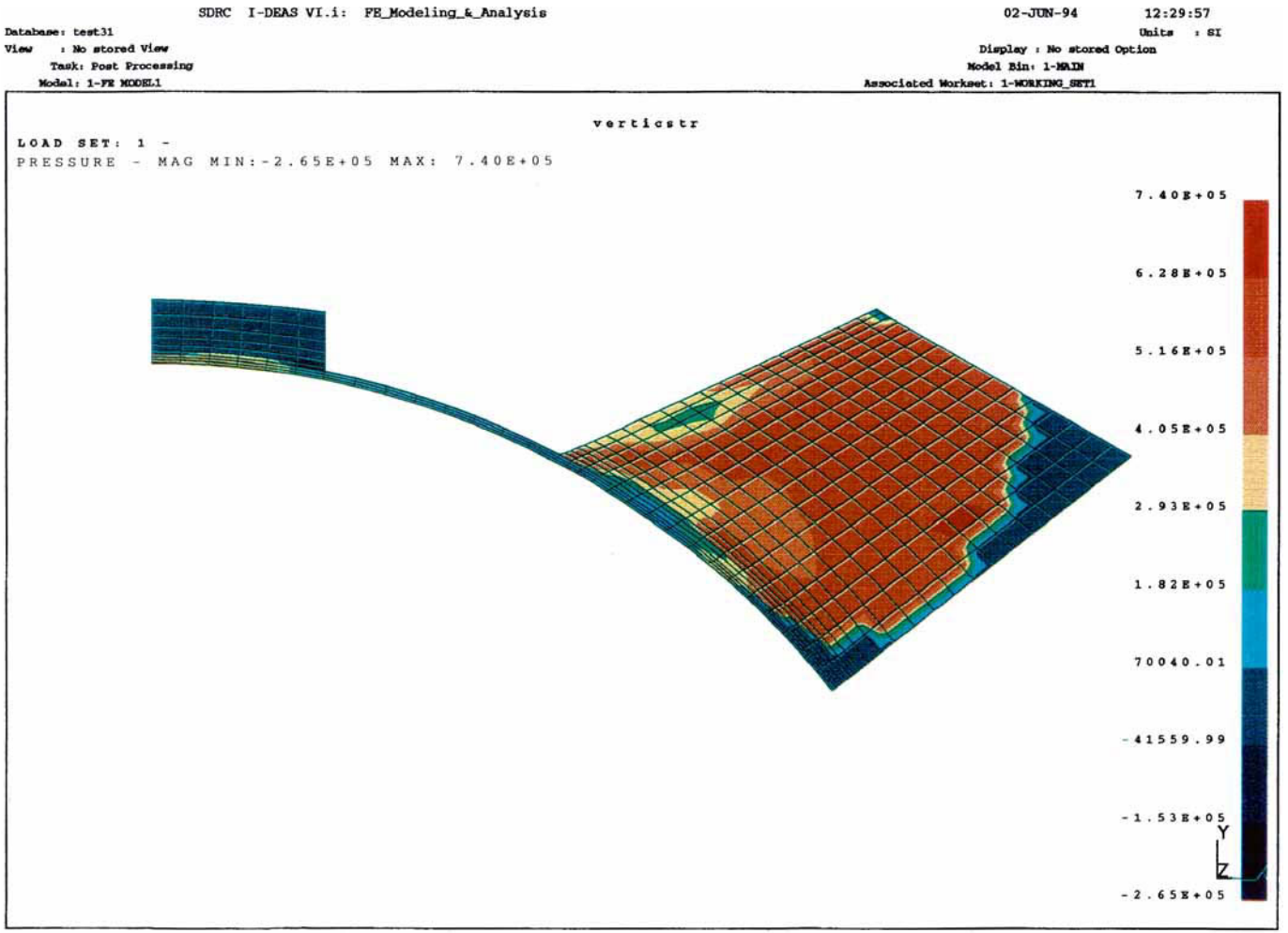

Plate 1. Simulated pressure contours 15s after start of flow in full reservoir experiment

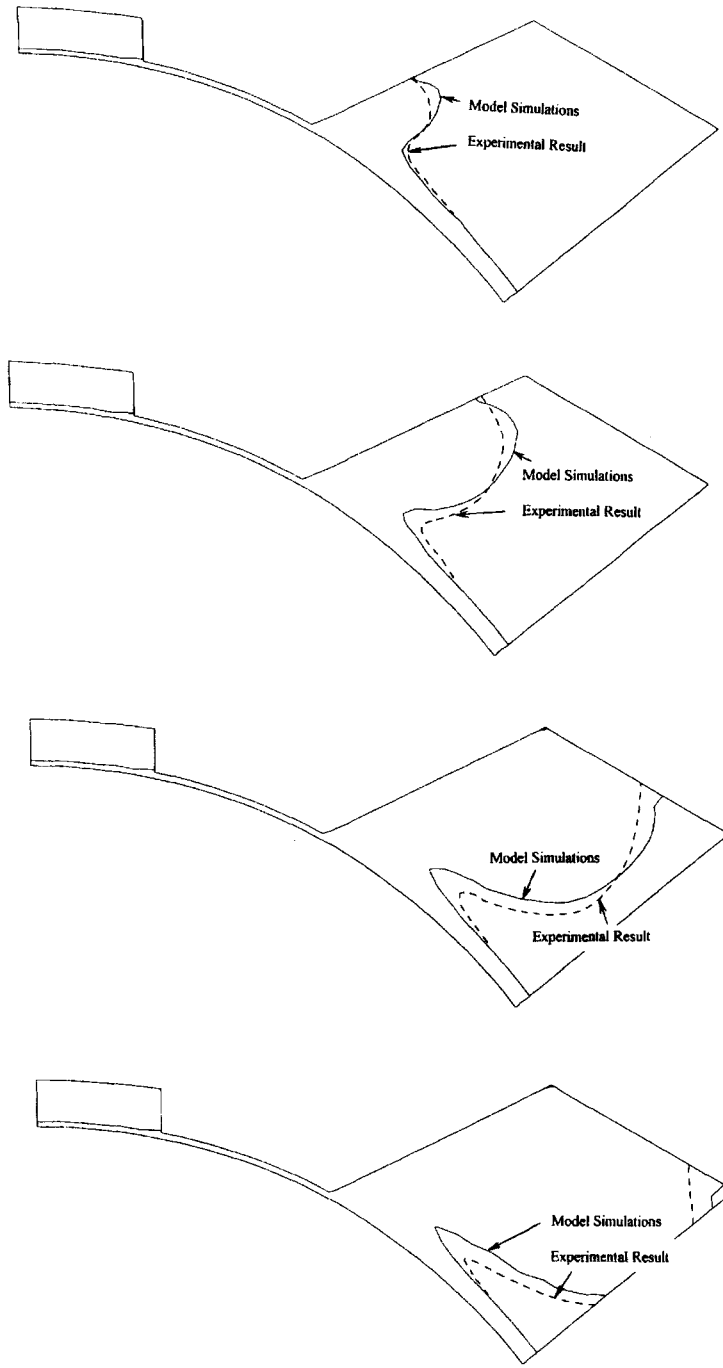

Figure 6. Comparison of numerically simulated free surfaces with experimental data (a) 5 s, (b) 15 s, (c) 40 s and (d) 55 s after start of flow

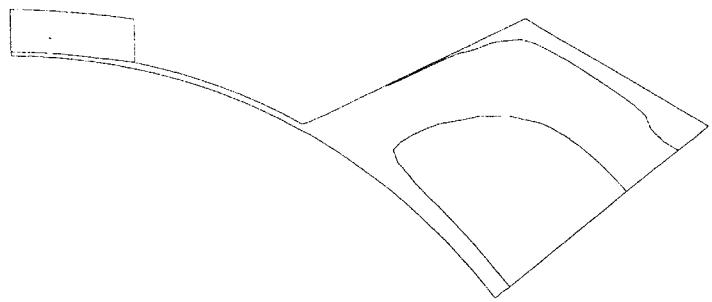

Figure 7. Simulated free surface location using traditional pseudodensity method

ACKNOWLEDGEMENT

The authors wish to express their gratitude to the Science and Engineering Research Council (U.K.) for a grant to support research work of which this study forms a part.

REFERENCES

1. B. D. Nichols, C. W. Hirt and R. S. Hotchkiss, 'SOLA-VOF: a solution algorithm for transient fluid flow with multiple free boundaries', *Los Alamos Scientific Laboratories Rep. LA-8355*, 1980.
2. W. S. Hwang and R. A. Stoehr, 'Molten metal flow prediction for complete solidification analysis of near net shape castings', *Mater. Sci. Technol.*, **4**, 240–250 (1988).
3. B. Minaie, K. A. Stelson and V. R. Voller, 'Fluid flow and solidification modelling of die castings', *ASME, Model. Mater. Process.*, **3**, 35–50 (1987).
4. E. Thompson, 'Use of pseudo-concentrations to follow creeping viscous flows during transient analysis', *Int. j. numer. methods fluids*, **6**, 749–761 (1986).
5. R. W. Lewis, A. S. Usmani and J. T. Cross, 'Finite element modelling of mould filling', in E. Onate, J. Periaux and A. Samuelsson (eds), *Finite Elements in 90s*, Springer/CIMNE, Barcelona, 1991.
6. O. C. Zienkiewicz and J. Wu, 'Incompressibility without tears; how to avoid restrictions of mixed formulations', *Int. j. numer. methods eng.*, **32**, 1189–1203 (1991).
7. S. Middleman, *Fundamentals of Polymer Processing*, McGraw-Hill, New York, 1977.
8. O. C. Zienkiewicz and R. L. Taylor, *The Finite Element Method*, Vol. 2, McGraw-Hill, London, 1991.
9. J. Donea and L. Quartapelle, 'An introduction to finite element methods for transient advection problems', *Comput. Methods Appl. Mech. Eng.*, **95**, 169–203 (1992).
10. R. B. Bird, R. C. Armstrong and O. Hasseger, *Dynamics of Polymer Liquids*, Vol. 1, Wiley, New York, 1987.
11. J. Petera and J. F. T. Pittman, 'Iso-parametric Hermite elements', *Int. j. numer. methods eng.*, **37**, 3489–3519 (1994).
12. V. Nassehi and J. Petera, 'A new least-squares finite element model for combined Navier–Stokes and Darcy flows in geometrically complicated domains with solid and porous boundaries', *Int. j. numer. methods eng.*, **37**, 1609–1620 (1994).
13. V. Nassehi and J. Petera, 'A new general purpose finite element model for steady incompressible low viscosity laminar flow using iso-parametric C^1 continuous Hermite elements', *Int. j. numer. methods fluids*, **18**, 215–226 (1994).